Supporting Text

^{14}C Uptake and Net Primary Production. Radiocarbon ^{14}C fixation is the standard method of estimating phytoplankton productivity. The ^{14}C method can, however, be estimating gross primary production (GPP), net primary production (NPP) or net community production (NCP) depending on the length of the incubation and on how much heterotrophic activity is occurring (1). Our NPP estimates are, in fact, net particulate carbon production [see discussion below on dissolveld organic carbon (DOC) production] and would be expected to match the primary production estimates based on ^{14}C uptake. But our estimated NPP significantly overestimates ^{14}C uptake (paired *t* test, t = 13.36, df = 145, $P << 0.001$). When we compared ^{14}C uptake to our estimate of NCP, there was no significant difference between the rates obtained by both methods (paired *t* test, t = 1.33, df = 105, $P = 0.19$). The comparison of NCP and ^{14}C uptake is counterintuitive because ^{14}C uptake can not be negative, whereas NCP sometimes is, but, nevertheless, good agreement is usually found between ^{14}C uptake and NCP measured by the light−dark O_2 method (1). The fact that GPP estimated following our application of the metabolic theory of ecology (MTE) and GPP measured by *in situ* light−dark bottle incubations agree relatively well supports the idea that something more than the many possible biases in our application of MTE (see below) might be responsible for the lack of agreement between NPP and ^{14}C uptake estimates.

Error Propagation. The errors in our estimates of community respiration (CR) and phytoplankton production obtained by using equations in Table 1 were

calculated through simulation, because it was not possible to do it analytically. For each station, 1,000 simulations were run and an estimate of the community metabolism obtained in each iteration. The error in the final estimate was obtained from the probability distribution of these simulations. In each iteration, a new equation was obtained by sampling a multivariate normal distribution with variance−covariance matrix equal to that of the model parameters in the initial fit. The metabolic rate of each individual was calculated by using this new equation, and a random normal deviate was added to each estimate.

Areal Estimates of Metabolic Balance. Our evaluation of the depth integrated balance using the MTE method is limited by sampling at only two or three depths for the determination of phytoplankton abundance. Sampling at two or three depths within the euphotic zone raises the possibility of biased integrated estimates if the depth of maximum production was not appropriately resolved (2). This bias is usually also the case of on-board incubations because of the limitation in the number of simulated light and temperature conditions that can be reproduced. The threshold depth integrated GPP for metabolic balance using the available data from Atlanctic Meridional transect (AMT) 1−6 cruises obtained by the MTE approach is 13.3 mmol of $O_2 \cdot m^{-2} \cdot d^{-1}$ (Fig. 7*A*) again within the lower range of depth integrated GPP threshold reported from *in situ* incubations (3–5). The exact value of the threshold GPP for metabolic equilibrium is, nevertheless, prone to statistical debate because some authors estimate its value from the ordinary least-squares relationship (OLS) between CR and GPP, whereas others use the reduced major axis regression (RMA) that would systematically yield a lower

threshold GPP. For example, the volumetric threshold GPP for metabolic equilibrium that can be obtained from the reported RMA regression on the global data set of respiration and production measurements (6) is 1.27 mmol of $O_2 \cdot m^{-3} \cdot d^{-1}$ while the OLS regression yields a threshold GPP of 1.47 mmol of $O_2 \cdot m^{-3} \cdot d^{-1}$. This effect is particularly accentuated when considering areal estimates because of the lower determination coefficient between CR and GPP and, therefore, the larger difference between OLS and RMA fits. By using the reported regression equations for the global data set (6), the integrated threshold GPP for metabolic equilibrium ranges from 106.42 mmol of $O_2 \cdot m^{-2} \cdot d^{-1}$ for the OLS fit to no existing threshold GPP because of the RMA fit having a slope of 1 and, hence, never crossing the 1:1 line. The areal and volumetric threshold GPP for metabolic balance obtained from the OLS fit to our MTE derived metabolic rates are 38.32 mmol of $O_2 \cdot m^{-2} \cdot d^{-1}$ and 0.71 mmol of $O_2 \cdot m^{-3} \cdot d^{-1}$ respectively. In any case, inspection of the geographical distribution of NCP (Fig. 7*B*) supports the hypothesis of prevailing net heterotrophy and plankton pelagic communities acting as CO_2 sources over the epipelagic oligotrophic regions of the Atlantic Ocean.

Caveats and Benefits of the MTE Estimation of the Metabolic Balance. The determination of the metabolic balance of the open ocean depends on proper spatial and temporal scale integration. The MTE models presented here would be restricted only by the number of plankton samples one can analyze for size structure either based on preserved samples or in near real-time. The growing use of automated counting and imaging instruments will, therefore, make our MTE models an increasingly practical option. The MTE models have the added

advantage that they can be applied to historical preserved samples or past data sets, further increasing the spatiotemporal scales of the measurement of metabolic balance in the upper oceans and improving our understanding of the global CO_2 budget. Also, the immediate fixation of a plankton sample upon collection avoids some problems of incubation methods due to artificial containment and manipulation of planktonic organisms and the need to maintain a temperature equal to that at which the water was collected, because a small rise in temperature can increase respiration, with subsequent errors in the interpretation of oceanic C flux.

Although there are no significant differences between our estimated GPP and GPP measured by *in situ* light−dark bottle incubations, the available data set of paired observations is still scarce and limited to relatively high GPP. Production of dissolved organic carbon (DOM) by phytoplankton was not taken into account in our GPP estimate. The percent extracellular release (PER) of DOC is usually close to $10-20\%$ (see ref. 7, and references therein). Further validation is required at low GPP, specially given that PER appears to be higher under more oligotrophic conditions (8, 9). The omission of PER from our calculations renders our threshold GPP for metabolic equilibrium an overestimation. If we estimate DOM production from our GPP using the empirical relationship in ref. 9 and add up DOM production to GPP in our calculations, the threshold GPP for metabolic equilibrium would be 0.25 mmol of $O_2 \cdot m^{-3} \cdot d^{-1}$ instead of the reported value of 0.4 mmol of $O_2 \cdot m^{-3} \cdot d^{-1}$ which, as mentioned before, already lies within the lower limit of threshold GPP reported from data on incubation measurements.

The contribution of inactive bacteria was also not assessed in our estimation of

oceanic community respiration. The dormant or stationary phases of these organisms appear to be significant in natural assemblages (10). Fortunately, there are promising techniques involving the flow−cytometric sorting of cells marked with various probes that can distinguish between inactive and active microbes (11). Hence, although in the work presented here, bacterial activity was not assessed, future developments may lead to a reduction of this potential error. The degree and sign of this error in our study can not be assessed precisely, because our sources for the individual bacteria respiration were determined by dividing bacterial CR by bacterial abundance, and we also lack knowledge about the fraction of inactive bacteria in those incubations.

Only one volume measurement was considered representative of all the individuals of a species in the AMT samples. This is an oversimplification, because cell volume and morphology can change during the cell cycle. With the use of automated and instantaneous counting and sizing instruments, the empirical models presented here can be applied to provide estimates of primary production and respiration rates with less potential error.

Furthermore, our first−order model does not intend to encompass all the sources of variability in the physiological rates of planktonic organisms (e.g., resource limitation, photoinhibition, photoacclimation, etc). Indeed, it should always be kept in mind that the normalization constants are subject to variation (12) both as a response to external factors and due to interspecific differences. As emphasized several times in the seminal work of MTE (13), it is not a “theory of everything”, but, as we have shown here for planktonic communities, it is able to make explicit

quantitative predictions, and we expect that the patterns in the residual variation not explained by the metabolic model would serve as hints for the possible causes.

Temperature dependence of the GPP:CR ratio. Following our application of MTE (Eqs. **1**−**4**), the GPP:CR ratio can be calculated as

$$GPP/CR = \frac{\frac{1}{V}\sum_{i=1}^{n_a} P_i}{\frac{1}{V}[\sum_{i=1}^{n_a}(1-\epsilon)P_i + \sum_{i=1}^{n_h} B_i]}. \quad [5]$$

Dividing the numerator and denominator by $\sum_{i=1}^{n_a} P_i$ and simplifying we get

$$GPP/CR = 1/[(1-\epsilon) + \frac{\sum_{i=1}^{n_h} B_i}{\sum_{i=1}^{n_a} P_i}], \quad [6]$$

which combined with eqs. **1** and **2** leads to

$$GPP/CR = 1/[(1-\epsilon) + \frac{b_0}{p_0} e^{(E_a - E_h)/kT} \frac{PAR + K_m}{PAR} \frac{\sum_{i=1}^{n_h} M_i^{\alpha_h}}{\sum_{i=1}^{n_a} M_i^{\alpha_a}}]. \quad [7]$$

This equation shows that the temperature−dependence of the GPP:CR ratio would be due solely to the differential individual-level activation energies of autotrophic and heterotrophic metabolism (E_a and E_h) if the other two terms in the equation, $\frac{PAR+K_m}{PAR}$ and $\frac{\sum_{i=1}^{n_h} M_i^{\alpha_h}}{\sum_{i=1}^{n_a} M_i^{\alpha_a}}$, were independent of temperature. From the AMT 1−6 data, we can see that, although the ratio between the heterotrophic and autotrophic size distributions, $\frac{\sum_{i=1}^{n_h} M_i^{\alpha_h}}{\sum_{i=1}^{n_a} M_i^{\alpha_a}}$, increases with temperature (*t* = -2.2, *df* = 158, $P = 0.03$, Fig. 8*A*), this increase is compensated by the decrease in the light dependence term with increasing temperature ($ln(\frac{PAR+K_m}{PAR}) = 0.15 * (1/kT) - 5.51$, $r^2 = 0.054$, *t* = 0.14, *df* = 158, $P = 0.003$) so that the product of both terms is in-

dependent of temperature (t = -0.3, df = 158, $P = 0.77$, Fig. 8*B*). If we subsitute in eq. **7** the estimated parameters for ϵ, b_0, p_0, and $E_a - E_h$ from our analysis (Table 1) and the average value for $\frac{PAR+K_m}{PAR}\frac{\sum_{i=1}^{n_h} M_i^{\alpha_h}}{\sum_{i=1}^{n_a} M_i^{\alpha_a}}$ of 1.76 from AMT $1-6$ data, we can see that this MTE$-$derived temperature$-$dependence of the GPP:CR ratio is well approximated by the simplified exponential temperature dependence term $e^{E_{a:h}/kT}$ (Fig. 8*C*).

Metabolic Balance Feedback on Climate Warming. Carbon dioxide is the greenhouse gas that most contributes to anthropogenic climate change. The oceans are an important sink for much of this CO_2. Understanding how future warming will affect this ocean sink is essential to improve the predictions of how climate will behave in the future. Climate change has already caused important changes on planktonic community composition and dynamics and these changes in community structure will likely modify the response of the ocean sink to future warming. In addition, global warming is predicted to become as large as 5.5 K when the carbon cycle is included in climate models compared with a 4 K increase in the uncoupled carbon models (14). But these coupled climate models do not consider the differential temperature response of the heterotrophic and autotrophic proccesses of the oceans' biota predicted by our theory. Our results suggest that the carbon$-$cycle feedback might have been underestimated because the oceans will capture less CO_2 with a future temperature increase (Fig. 9*A*). An increase in global temperature will drive the metabolic balance of the oceans towards heterotrophy, reducing the ocean sink and increasing the levels of atmospheric CO_2, which will, in turn, close the feedback loop by a further increase in

global warming. To estimate the magnitude of this reduction in the ocean carbon sink, we combined current global estimates of epipelagic ocean respiration and production (15) with our temperature−dependence equations. A global estimate (G) will increase with temperature according to

$$G = G_c e^{(E/k)(1/T - 1/(T+\Delta T))}, \quad [8]$$

where G is the global rate (i.e. production or respiration) under a temperature − increase scenario ΔT, E is the respective activation energy and G_c and T are the current global rate and temperature.

The predictions of the global temperature rise over the 21st century are necessarily uncertain and are dependent on the different CO_2 emission scenarios. Ocean temperatures will follow a similar increase to that in the atmosphere (16). For an average temperature increase of 3°C, the metabolic balance dependence on temperature would cause a reduction of 22% less CO_2 captured (Fig. 9*A*), equivalent to one-third of the current worldwide CO_2 emissions by industrial activities (Intergovernmental Panel on Climate Change (IPCC) Special Report on Carbon Dioxide Capture and Storage, Fig. 9*B*; the solid line in Fig. 9*B* is the metabolic balance decrease for the central global production and respiration estimates reported in ref. 15 whereas the dashed and dotted lines are the predictions for the low and high estimates of global rates, see Table 1 in ref. 15). For the full range of 35 emission scenarios reported by the IPCC (17) the globally averaged surface temperature is predicted to increase by between 1.4°C and 5.8°C.

This temperature rise will cause a reduction in the metabolic balance between 1.7 and 10.4 Gigatons $C \cdot yr^{-1}$, which represents between 12% and 77% of current yearly worlwide CO_2 emissions from industrial activities (Fig. 9*B*). Therefore, the change of the metabolic balance with global warming can be a highly relevant feedback. There are, however, many other responses of marine ecosystems to climate change (18–21). Moreover, there is an upper limit to heterotrophy set by the inputs of allochthonous carbon, because respiration cannot exceed the sum of GPP + allochthonous organic carbon inputs. Obtaining a realistic prediction of the effects of climate change on plankton communities is not as simple as the first−order calculations provided here. Our calculations are, rather, intended to show that, because the direct effects of temperature on the metabolic balance can be potentially important, they should be taken into account in future improvements of coupled carbon−climate models.

References

1. Marra, J. (2002) in *Phytoplankton Productivity: Carbon Assimilation in Marine and Freshwater Ecosystems*, eds. le B. Williams, P. J., Thomas, D. N. & Reynolds, C. S. (Blackwell Scientific, Oxford), pp. 78–108.

2. Robinson, C., Serret, P., Tilstone, G., Teira, E., Zubkov, M. V., Rees, A. P. & Woodward, E. M. S. (2002) *Deep-Sea Res.* **49**, 787–813.

3. Serret, P., Fernandez, E. & Robinson, C. (2002) *Ecology* **83**, 3225–3234.

4. Serret, P., Robinson, C., Fernandez, E., Teira, E. & Tilstone, G. (2001) *Limnol. Oceanogr.* **46**, 1642–1652.

5. Duarte, C. M., Agustí, S., Arístegui, J., González, N. & Anadón, R. (2001) *Limnol. Oceanogr.* **46**, 425–428.

6. Robinson, C. & le B. Williams, P. J. (2005) in *Respiration in Aquatic Ecosystems*, eds. del Giorgio, P. & le B. Williams, P. J. (Oxford Univ. Press, Oxford), pp. 147–180.

7. Nagata, T. (2000) in *Microbial Ecology of the Oceans*, ed. Kirchmann, D. L. (Wiley-Liss, New York), pp. 121–152.

8. Teira, E., Serret, P. & Fernandez, E. (2001) *Mar. Ecol. Prog. Ser.* **219**, 65–83.

9. Morán, X. A. G., Estrada, M., Gasol, J. M. & Pedrós-Alió, C. (2002) *Microb. Ecol.* **44**, 217–223.

10. Smith, E. M. & del Giorgio, P. A. (2003) *Aquat. Microb. Ecol.* **31**, 203–208.

11. Zubkov, M. V., Fuchs, B. M., Tarran, G. A., Burkill, P. H. & Amann, R. (2002) *Aquat. Microb. Ecol.* **29**, 135–144.

12. Niklas, K. J. (2004) *Biol. Rev. Cambridge Philos. Soc.* **79**, 871–889.

13. Brown, J. H., Gillooly, J. F., Allen, A. P., Savage, V. M. & West, G. B. (2004) *Ecology* **85**, 1771–1789.

14. Cox, P. M., Betts, R. A., Jones, C. D., Spall, S. A. & Totterdell, I. J. (2000) *Nature* **408**, 184–187.

15. del Giorgio, P. A. & Duarte, C. M. (2002) *Nature* **420**, 379–384.

16. Plattner, G. K., Joos, F., Stocker, T. & Marchal, O. (2001) *Tellus* **53B**, 564–592.

17. Houghton, J. T., Ding, Y., Griggs, D. J., Noguer, M., van der Linden, P. J., Dai, X., Maskell, K. & Johnson, C. A., eds. (2001) *Climate Change 2001: The Scientific Basis. Contribution of Working Group I to the Third Assessment Report of the Intergovernmental Panel on Climate Change*. (Cambridge Univ Press, Cambridge, U.K.).

18. Sarmiento, J. L. & LeQuere, C. (1996) *Science* **274**, 1346–1350.

19. Edwards, M. & Richardson, A. (2004) *Nature* **430**, 881–884.

20. Hays, G. C., Richardson, A. J. & Robinson, C. (2005) *Trends Ecol. Evol.* **20**, 337–344.

21. Beardall, J. & Raven, J. A. (2004) *Phycologia* **43**, 26–40.

Figure 5. (**A**), Effects of body volume on temperature corrected respiration rates of bacteria (triangles) and micro- and meso-zooplankton (squares and crosses). (**B and C**), effects of cell volume on phytoplankton respiration (**B**) and production (**C**) corrected for the effects of temperature and light.

Figure 6. Tracks for the Atlantic Meridional Transect cruises (AMT 1-6).

Figure 7. (**A**), The relationship between areal estimates of gross primary production (GPP) and community respiration (CR) estimated based on metabolic theory. Solid line is the reduced major axis relationship. Dashed line is the 1:1 relationship. The GPP where both lines intersect is the threshold GPP for metabolic balance (GPP=CR). (**B**), Map showing the geographical distribution of plankton metabolic balance estimated using the allometric method. Locations with negative net community production (NCP=GPP-CR) (blue squares) are net sources of CO2 while red open circles represent locations where the planktonic community is net autotrophic (NCP¿0).

Figure 8. (**A**), Temperature dependence of the size distribution ratios for autotrophs and heterotrophs $\frac{\sum_{i=1}^{n_h} M_i^{\alpha_h}}{\sum_{i=1}^{n_a} M_i^{\alpha_a}}$ from AMT 1-6. (**B**), lack of temperature dependence of the term $\frac{\sum_{i=1}^{n_h} M_i^{\alpha_h}}{\sum_{i=1}^{n_a} M_i^{\alpha_a}}$ multiplied by (PAR+Km)/PAR for the AMT 1-6. (**C**), temperature dependence of the GPP : CR ratio obtained using the global dataset as also shown in Fig. 4 B. Solid line is the ordinary least square relationship. Red line is the MTE-predicted response from the full model presented in the Supplementary Information.

Figure 9. (**A**), Decrease in the metabolic balance of the oceans (black solid line) with the sea surface temperature increase (dotted blue line) predicted by the

Community Climate System Model (CCSM) of the National Center for Atmospheric Research (NCAR) under IPCC scenario A2 for the twenty first century. (**B**), Metabolic balance decrease (left axis) and percentage of current yearly worlwide CO2 emissions by industrial activities this change represents (right axis) for the full range of temperature increase predicted under the 35 emission scenarios reported by the Intergovernmental Panel on Climate Change. The solid line is the metabolic balance decrease for the central estimates of global production and respiration while the dashed and dotted lines are the predictions for the low and high estimates of global rates (see Supplementary text).

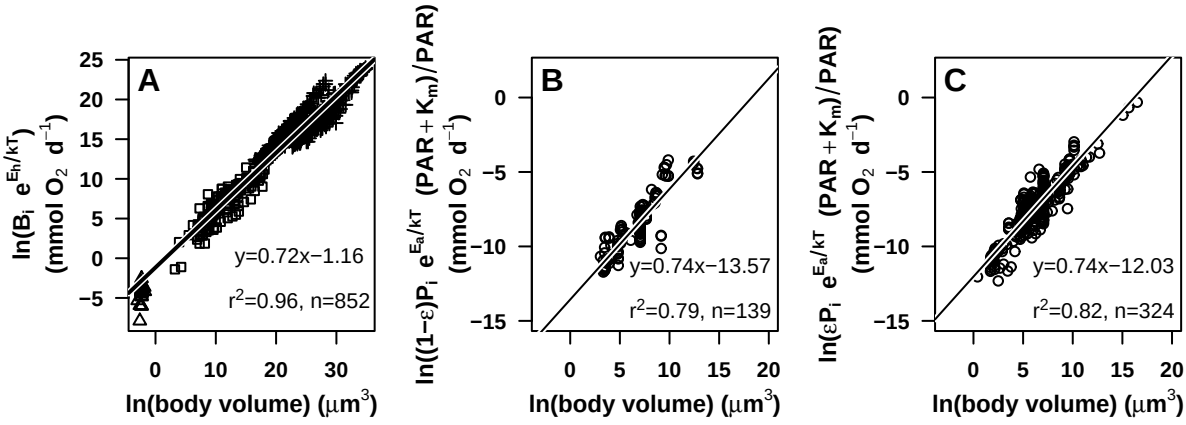

Figure 5: Lopez-Urrutia et al

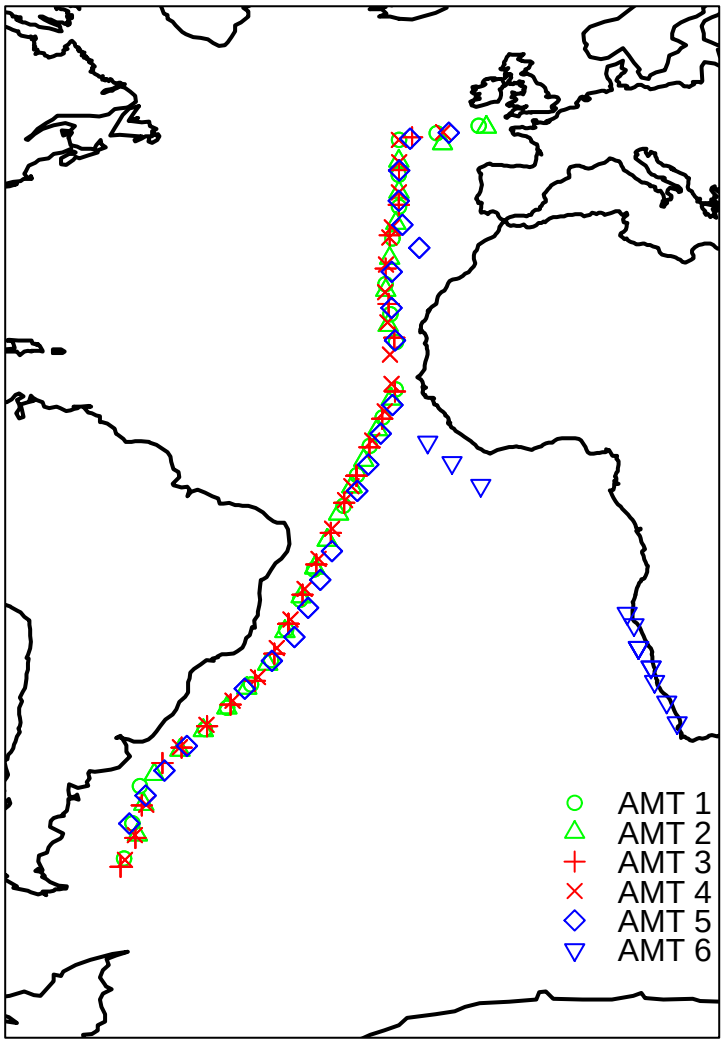

Figure 6: Lopez-Urrutia et al

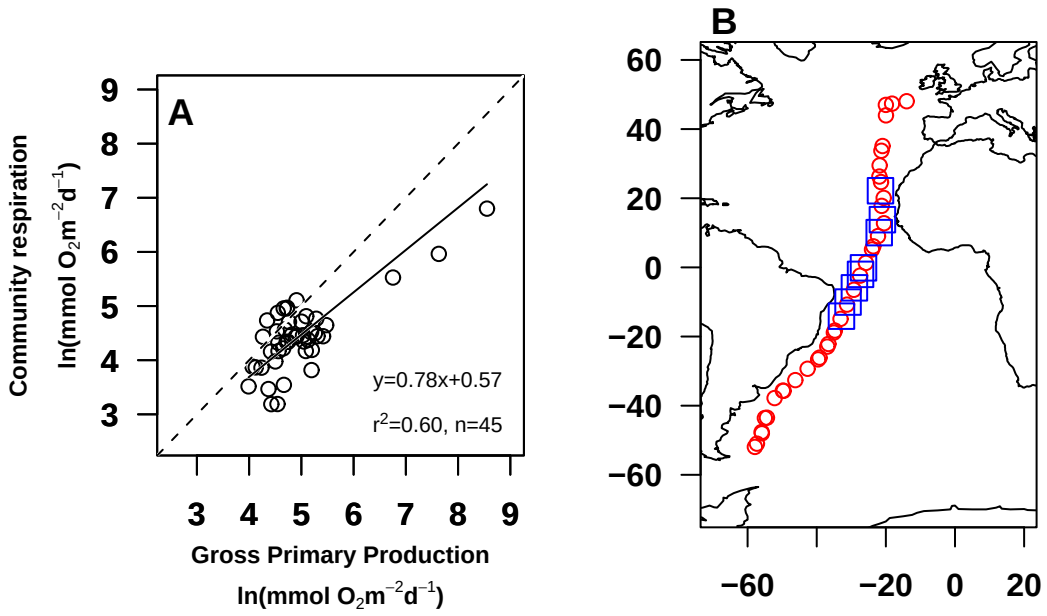

Figure 7: Lopez-Urrutia et al

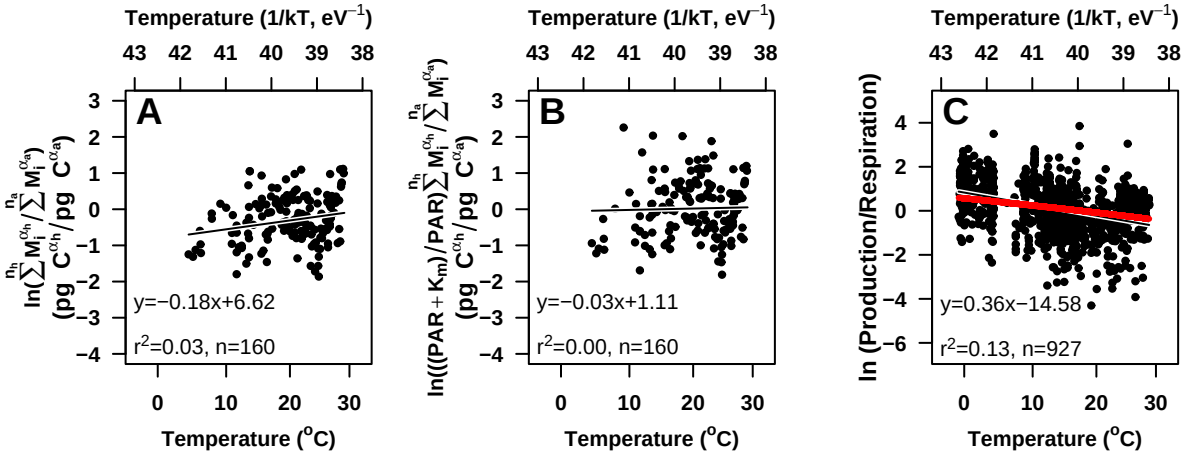

Figure 8: Lopez-Urrutia et al

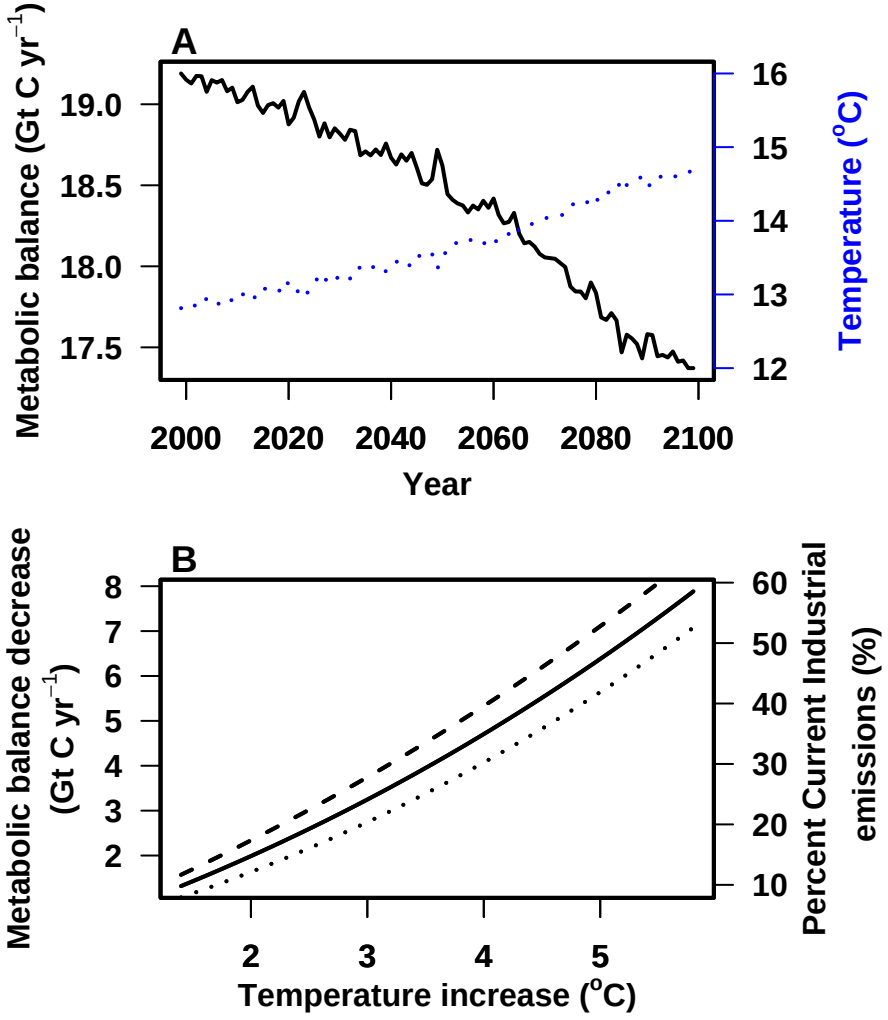

Figure 9: Lopez-Urrutia et al